

Assessment of Remote Data Capture Systems for the Characterisation of Rock Fracture Networks within Slopes


Xander P Gwynn

Camborne School of Mines
School of Geography Archaeology and Earth Resources
University of Exeter

Submitted by Xander Peter Gwynn to the University of Exeter as a thesis for the degree of Doctor of Philosophy in Earth Resources, September, 2008.

This thesis is available for Library use on the understanding that it is copyright material and that no quotation from the thesis may be published without proper acknowledgement.

I certify that all material in thesis which is not my own work has been identified and that no material has previously been submitted and approved for the award of a degree by this or any other University.


..... (signature)

ABSTRACT

The use of remote techniques to capture the geometrical characteristics of rock masses has seen increased use and development in recent years. Apart from the obvious improved Health and Safety aspects, remote techniques allow rapid collection of digital data that can be subsequently analysed to provide input parameters for a variety of geomechanical applications. Remote data capture is a new technique used to collect geotechnical data and little independent work has been done concerning the comparative limitations and benefits of photogrammetry and laser scanning. Photogrammetry and laser scanning produce three dimensional digital representations of a studied rock face which can then be mapped for geotechnical data using specialist software.

Research conducted at Camborne School of Mines, University of Exeter has focussed on developing robust and flexible methodologies for remote data capture techniques, namely photogrammetry and laser scanning. Geotechnical characterisation for photogrammetry was tested using the CSIRO Sirovision software and laser scanning was used with SplitFX from Split Engineering. A comparative method of assessing the error between orientation measurements was developed based on calculating the pole vector difference between remotely captured and traditionally hand-mapped data. This allowed for testing of the benefits of the remote data capture systems and limitations whilst comparing them with conventional hand-mapping. The thesis also describes the results of detailed comparisons between hand-mapping, photogrammetric and laser scanned data collection for discontinuity orientation, roughness, discontinuity trace lengths and potential end-use applications.

During fieldwork in Cornwall, Brighton Cliffs and northern France it was found that remote data capture techniques struggled to collect orientation data from intensely fractured rock masses where features are primarily represented as discontinuity traces.

It was found that both photogrammetry and laser scanning produce orientation data comparable to traditionally mapped data, with an average pole vector difference less than 12° from data mapped from the Tremough Campus road cutting to the University of Exeter's Cornwall Campus. Set analysis on 151 comparable data points yielded a maximum set pole vector difference of 9.8° , where the closest difference was 2.24° . Testing the accuracy of discontinuity trace orientations captured by photogrammetry

using the pole vector difference methods indicate that planar derived orientations are more accurate, with an average difference of 16.67° compared to 37.72° .

This thesis contains the reviews and analyses of photogrammetry and laser scanning for use in characterising natural and manmade rock slopes. Improved field and post-processing methodologies have been developed to aid the safe, efficient and suitable geotechnical characterisation of rock fracture networks. The continual development and use of remote mapping techniques, whilst supplementing their unique qualities with traditional mapping, have the capability to revolutionise rock mass mapping. Particular development needed is the implementation of ISRM guidelines to standardise photogrammetric and laser scanning fieldwork and post-processing data analysis.

CONTENTS

Abstract	2
Contents	4
List of Figures	8
List of Tables	18
Acknowledgements	21
1 Introduction	22
1.1 Aims of Project	24
1.2 Outline of Thesis	26
2 Remote Data Capture	28
2.1 Remote Sensing.....	28
2.2 Photogrammetry.....	29
2.2.1 History	29
2.2.2 Photogrammetric Systems.....	30
2.2.3 Photogrammetric Principles	30
2.3 Laser Scanning	32
2.3.1 History	32
2.3.2 Laser Scanning Systems	33
2.3.3 Laser Scanning Principle	33
2.4 Uses of Remote Data Capture.....	35
2.4.1 Geotechnical Aspects.....	35
2.4.2 Coastal Geotechnical Aspects	36
2.4.3 Non-Geotechnical.....	37
2.5 Review of Previous Work Undertaken	38
2.6 Summary.....	43
3 Data Capture Process Work-flow	44
3.1 Introduction	44
3.2 Workflow Sections Overview	46
3.2.1 Planning	46
3.2.2 On Site Assessment.....	46
3.2.3 Positioning.....	46
3.2.4 Data Capture	47
3.2.5 Data Capture / Data Compilation	47
3.2.6 Data Output / Analysis	48
3.2.7 End-Use Applications	48
3.3 Planning	48

3.3.1	Distance to Face and Study Area	48
3.3.2	Camera Separation / Baseline Ratio (Photogrammetry)	49
3.3.3	Orientation to Face	50
3.3.4	Geology of the Studied Rock Face	51
3.3.5	Equipment and Software Cost	56
3.4	On site Assessment	57
3.4.1	Camera Lens.....	57
3.4.2	Access.....	57
3.4.3	Atmospheric Conditions.....	57
3.4.4	Speed / Time	58
3.5	Positioning.....	58
3.5.1	Compass Clinometer and Tape Measure	58
3.5.2	Global Positioning System (GPS)	60
3.5.3	Differential GPS.....	61
3.5.4	Reflectorless Total Station.....	63
3.6	Data Capture.....	64
3.6.1	Photogrammetry	64
3.6.2	Laser Scanning	66
3.6.3	Traditional Hand-mapping Combined with Digital Photography	69
3.7	Photogrammetric 3D Image and Point Cloud Creation	72
3.7.1	Photogrammetric 3D image Creation.....	72
3.7.2	Laser Scanning Point Cloud Creation.....	76
3.8	Processing and Analysis of Remotely Captured Data.....	76
3.8.1	Data Import.....	76
3.8.2	Sirojoint and SplitFX Processing.....	77
3.9	End-Use Applications	82
3.10	Discussion and Conclusion	82
3.10.1	Fieldwork processes.....	82
3.10.2	Post-Processing/Data Analysis	84
4	Assessment of Fieldwork and Mapping Processes.....	86
4.1	Introduction	86
4.2	Pole Vector Difference.....	88
4.2.1	Pole Vector Difference Calculations	88
4.2.2	Pole Vector Difference of Hand-mapping.....	91
4.2.3	Interpretation of Pole Vector Difference Values	91
4.3	Area of Face Analysis	91
4.3.1	Photogrammetry.....	95

4.3.2	Laser Scanning	98
4.3.3	Orientation Data	99
4.3.4	Pole vector difference analysis	103
4.4	Rock Type/Structure Analysis.....	104
4.4.1	Gwithian and Gunwalloe Cliffs.....	105
4.4.2	Portreath Cliff	113
4.4.3	Porthgwarra, Carn Marth Quarry and Theatre Quarry.....	115
4.4.4	Portobello Cliffs	125
4.4.5	Assessment of Remote Data Capture to Collect Data from Varying Rock Types/Structures.....	126
4.5	Baseline to Face Ratio Analysis	127
4.6	Baseline Orientation to Face Analysis	131
4.7	Distance to Face Analysis	133
4.7.1	Imerys – Blackpool Pit.....	133
4.7.2	Delabole Quarry	136
4.7.3	Camborne School of Mines’ Test Mine	140
4.8	Equipment and Software Cost Analysis.....	143
4.9	Camera Lens Analysis.....	144
4.10	Access Analysis	144
4.10.1	Vegetation / Obstructions	144
4.10.2	Water Reflection.....	146
4.10.3	Rock Mesh	147
4.10.4	Blinding.....	149
4.11	Atmospheric Conditions.....	152
4.12	Field Speed / Time	154
4.13	Development of Positional Techniques.....	156
4.13.1	Compass Clinometer / Tape Measure.....	157
4.13.2	Global Positioning Systems / Differential Global Positioning Systems	157
4.13.3	Total Station	158
4.14	Development of Remote Data Capture /Data Compilation.....	158
4.14.1	Photogrammetry	158
4.14.2	Laser Scanning.....	160
4.14.3	Set Analysis.....	161
4.15	Summary.....	161
4.15.1	Pole Vector Difference.....	161
4.15.2	Scale	162
4.15.3	Impact of Lithology/GSI	162

4.15.4	Set-up Variations Affecting Data Capture	163
4.15.5	Distance	164
4.15.6	Costs	165
4.15.7	Access.....	165
4.15.8	Environmental and Timing Considerations.....	165
4.15.9	Image Processing.....	165
5	Data Output / Analysis Processes	167
5.1	Introduction	167
5.2	Tremough Campus Road Cutting Overview	169
5.2.1	Road Cutting Geographical Location and Geology	169
5.3	Orientation Comparison.....	176
5.3.1	Individual Feature	176
5.3.2	Set Comparison.....	177
5.4	Trace Analysis.....	180
5.4.1	Trace Orientation Analysis.....	180
5.4.2	Discontinuity Trace Length Analysis	181
5.5	Roughness Analysis.....	184
5.5.1	Conversion between Roughness Measurements.....	184
5.5.2	Using Profiles to Characterise Roughness	187
5.5.3	Scale of Roughness Affecting Orientation measurements	189
5.6	Tailoring Data for End-Use Applications	192
5.6.1	Geotechnical/Geological Data	193
5.6.2	RMR, Q System and GSI Ratings.....	202
5.6.3	Digital Elevation Model Data.....	203
5.6.4	Visual Data	209
6	Discussion.....	213
6.1	Introduction	213
6.1.1	Field and Mapping Processes.....	213
6.1.2	Data Output / Analysis Processes	216
6.2	Further Work	223
7	Conclusions	226
7.1	Key Findings	226
7.2	Summary.....	229
8	References	232

LIST OF FIGURES

Figure 2-1. Geometry for the determination of the position of a point in object space (from CSIRO, 2005).....	32
Figure 3-1. Process work-flow diagram with key underneath. The first stage requires that each parameter is considered before the site investigation starts, this can take place before or once the site is reached. The second stage uses an on site assessment to ascertain the conditions under which the remote data capture systems are to be used. The positioning technique is directly related to the data capture system used i.e. the tape measure and compass clinometer cannot be used to position the laser scanner. Once the data capture is completed the data is compiled using the programs specified. The dashed lines indicate that the photogrammetric/Sirovision process, once moved to data analysis, must be re-submitted into Sirovision to allow for the additional analysis facility to be used. The data analysis for all three techniques uses DIPS (Rocscience, 2006), however it is also used to compile the data for hand-mapping. Once the data is processed into spacing and roughness data, etc. it is available for use in the multiple end-uses.	45
Figure 3-2. Diagram showing scale effects upon overall rock mass strength. Capturing the rock mass characteristics at multiple scales is beneficial to geotechnical studies, as then instabilities of varying size can be factored into the analysis (from Wyllie & Mah, 2004).	49
Figure 3-3. Camera separation/ distance from face ratio. Cameras are orientated so that that the control point is in the centre of their view and spaced at a distance 1/6 of the baseline distance to the study face (modified from Siro3D manual, CSIRO, 2005).	50
Figure 3-4. Diagram showing potential distortion effects due to 'blinding'. Due to an unfavourable orientation/position of the camera or scanner, sections of the face are unseen. Photogrammetric 3D image creation will distort the final model to fit the data in view (blocked by the red section), where laser scan point clouds will have the red section missing (not to scale).....	51
Figure 3-5. Schematic from positional calculation sheet (eastings and northings). The schematic is used to visually assess the calculated locations for any gross errors, e.g. large camera separation or incorrect baseline to face orientation.	59
Figure 3-6. Magellan eXplorist handheld GPS. The GPS internal clock was synchronised with the clock of the camera/scanner, so to provide the most accurate positional data. The positional data can then be read off the screen or saved onto a GPS memory card (modified from www.magellangps.com).	60

Figure 3-7. Differential GPS Equipment – base station. The base station is setup over a known position that has previously been surveyed and begins to receive satellite signals. The location of the base station is input into the machine so it can then compare it with the positions that it calculates for itself using the satellite code, hence calculating the positional error for each moment in time. This error is then transmitted to the roving GPS unit so that it can calculate its position accurately.	61
Figure 3-8. Diagram showing the principle of Differential GPS.....	62
Figure 3-9. Roving GPS unit in backpack.....	62
Figure 3-10. TPS1200 reflectorless total station (from Leica, 2005).	64
Figure 3-11. Leica HDS3000 (from Leica, 2005). The laser is emitted through main window (pictured). A second window at the back of the scanner is used for capturing points at an angle of less than 40° from vertical.....	67
Figure 3-12. Photograph showing the Leica HDS4500 phase shift laser scanner. A mirror in the centre of the scanner spins reflecting the laser emitted vertically from the base of the scanner.	68
Figure 3-13. Schematic showing relative camera positions using Siro3D (CSIRO, 2006). Each camera position is labelled corresponding to the file name of the image on the computer. The blue rectangles show the extent of the photographs and how they relate to one another, along with the red cross indicating the control points and its location in the two images. This schematic allows for a visual assessment of the survey data.	74
Figure 3-14. Image showing result of poor matching of an underground rock face (~3 m wide) with multiple drill holes. The red box outlines the worst affected area of poor matching, however it is poor across the majority of the rock face. It is considered that this 3D image is poorly interpolated due the poor lighting and the multiple dark drill holes on the face which are incorrectly matched between the stereographic pair.	75
Figure 3-15. Post matching 3D mesh representing a full georeferenced rock face using Siro3D (CSIRO, 2005). Options are given for: manual editing of the 3D image, removing outliers automatically, cleaning up borders (by cropping), restoring original data (if one of the previous three options has already been applied), and to continue to save the 3D image.....	76
Figure 3-16. Full point cloud of example quarry (Carnsew) (red box, 6 m high, shows area required for analysis). The point clouds produced commonly contain points from areas that do not need to be analysed. They can be easily deleted from the point cloud file.....	79
Figure 4-1. Process work-flow diagram - indication of sections covered in Chapter 4.	87

Figure 4-2. Example stereonet shows differences in poles between hand (red), laser (green) and photogrammetric (blue) mapping. Each cluster of poles represents one discontinuity whilst each mapping technique has a slightly different orientation measurement.....	88
Figure 4-3. Diagram showing dip / dip direction conversion to Cartesian coordinates.	89
Figure 4-4. Map of Southern England, UK, showing location of Saltdean and Portobello coastal cliffs. © Crown Copyright/database right 2009. An Ordnance Survey/EDINA supplied service.	92
Figure 4-5. Geological map showing location of Portobello Cliffs (from Mortimore <i>et al.</i> , 2004).	92
Figure 4-6. Map showing photogrammetry study area and locations of laser scanner setup positions. © Crown Copyright/database right 2009. An Ordnance Survey/EDINA supplied service.	93
Figure 4-7. Image of cliff face at Portobello, UK, looking NE (30 m high).	94
Figure 4-8. Point cloud image (looking NW) showing area covered by two laser scans, 3 photogrammetric models (blue) and traditional hand-mapping (red) during morning visit (black line showing location of largest feature identified).....	94
Figure 4-9. Orthoimage (striking 085°) showing large scale structures (>1 m, blue) and small scale structures (<1 m, red).	97
Figure 4-10. Photograph showing small scale fractures found within the Portobello chalk (0.5 m high), looking north. The nodules within the chalk are flint and chert.	98
Figure 4-11. Point cloud showing large scale planes identified within SplitFX (red), Portobello Cliffs, Brighton, UK (30 m high), looking NE.....	99
Figure 4-12. Lower hemisphere representations showing contoured hand-mapped data taken from Portobello Cliffs, Brighton, UK (1 m - 30 m length), Lawrence (2007) (dip/dip direction of contour highs given in degrees). These large scale structures are predominantly steeply dipping and striking NE – SW, and NW – SE.....	100
Figure 4-13. Lower hemisphere stereonet showing contoured data from the SplitFX mapped point clouds, Portobello Cliffs, Brighton, UK (dip/dip direction of contour highs given in degrees). Similarly to hand-mapping, laser scanning only picks up the large scale features. The steeply dipping NE – SW, and NW – SE structure are identified, but a strong E – W striking set is also identified.	100
Figure 4-14. Lower hemisphere stereonet showing contoured orientation data from the large scale models, Portobello Cliffs, Brighton UK (dip/dip direction of contour highs given in degrees). The data is scattered but shows a similar NE – SW and NW – SE striking sets as hand-mapping.	101

Figure 4-15. Lower hemisphere stereonet showing contoured orientation data from the medium scale models, Portobello Cliffs, Brighton UK (dip/dip direction of contour highs given in degrees). The NW – SE striking set is clearly shown in the stereonet, although the NE – SW striking set is less apparent.	101
Figure 4-16. Lower hemisphere stereonet showing contoured orientation data from the small scale models, Portobello Cliffs, Brighton UK (dip/dip direction of contour highs given in degrees). The data is highly scattered and only weakly show the NE – SW and NW – SE striking sets identified from the large scale laser scanning and photogrammetric models.	101
Figure 4-17. Map of West Cornwall, UK, showing location of Gwithian and Gunwalloe cliffs. © Crown Copyright/database right 2009. An Ordnance Survey/EDINA supplied service.	105
Figure 4-18. Map showing photogrammetric study area at Gwithian cliffs. © Crown Copyright/database right 2009. An Ordnance Survey/EDINA supplied service.	106
Figure 4-19. Photograph of cliff face (~10 m high) at Gwithian, UK, looking east. The Variscan fold structures can be clearly seen within the face along with the complex jointing set orientations.	106
Figure 4-20. Lower hemisphere stereonet showing Gwithian orientation data.....	108
Figure 4-21. Equal area stereograms showing orientation data for: (a) Zones of distributed D3 shear, (b) D3 detachments, (c) D3 brittle listric extensional faults and (d) post D3 faults (from Alexander and Shail, 1995).....	108
Figure 4-22. Map showing location of photogrammetry study area at Blue Rocks, Gunwalloe. © Crown Copyright/database right 2009. An Ordnance Survey/EDINA supplied service.....	110
Figure 4-23. Photograph of cliff face at Blue Rocks, Gunwalloe, UK, looking north (cliff height from beach is 12 m). Folding is evident in the centre of the photograph, and wedge failures can be seen in the upper sections of the face.	110
Figure 4-24. Low angle detachments (faults) identified from the 'Big Wedge' model at Loe Bar, Gunwalloe (3 m high face, looking east). Using a visual assessment of separation and movement across discontinuity features, the faults were identified and mapped using the photogrammetric software.	111
Figure 4-25. Stereonet showing fault poles and associated slickenline data for the Loe Bar Lodge to Gunwalloe coastal section (from Shail & Wilkinson, 1994) (left) and the equivalent photogrammetrically mapped data (right).....	112
Figure 4-26. Map of West Cornwall, UK, showing location of Portreath. © Crown Copyright/database right 2009. An Ordnance Survey/EDINA supplied service.	113

Figure 4-27. Map showing location of laser scanning study area at Portreath. © Crown Copyright/database right 2009. An Ordnance Survey/EDINA supplied service. 114

Figure 4-28. Point cloud image showing identified large scale discontinuities (highlighted red) at Portreath beach cliff (15 m height) and failure material. The laser scan data also has the potential to be used to calculate the volume of the failed mass. 115

Figure 4-29. Map of West Cornwall, UK, showing location of Porthgwarra. © Crown Copyright/database right 2009. An Ordnance Survey/EDINA supplied service. 116

Figure 4-30. Map showing locations of photogrammetry study areas at Porthgwarra. © Crown Copyright/database right 2009. An Ordnance Survey/EDINA supplied service. 116

Figure 4-31. Photogrammetric orthoimage (striking E -W, 4 m high) showing discontinuity mapping at Porthgwarra Cliff, Cornwall, UK. Three roughly orthogonal discontinuity sets can be identified from the orthoimage. 117

Figure 4-32. Lower hemisphere stereonet from orientation data collected from Porthgwarra photogrammetric model. The three roughly orthogonal discontinuity sets identified from the orthoimage can be seen (delineated in red). The N - S striking set fluctuates cross the vertical, and can be separated into easterly and westerly dipping sub-sets. 118

Figure 4-33. Map of West Cornwall, UK, showing location of Carn Marth Quarry and Theatre Quarry. © Crown Copyright/database right 2009. An Ordnance Survey/EDINA supplied service. 120

Figure 4-34. Laser scan point cloud showing rock face at Carn Marth Quarry, Cornwall, UK, (5 m high, looking north) The blocky nature of the rock mass displays the discontinuities clearly. Sub horizontal features can also be identified. 121

Figure 4-35. 3D image screen capture of mapped rock face at Carn Marth Quarry with colours indicating similarly orientated discontinuities (scale shown in images, looking north). Similarly to the laser scanned point cloud, discontinuities are easily identified from the 3D model. 121

Figure 4-36. Map of Carn Marth and Theatre Quarries, stereonet representing each mapping type and location with set windows and major planes delineated in red. Photogrammetry = blue circles, laser scanning = green triangles and hand-mapping = red squares. © Crown Copyright/database right 2009. An Ordnance Survey/EDINA supplied service. 123

Figure 4-37. Map of West Cornwall, UK, showing location of Penlee Quarry. © Crown Copyright/database right 2009. An Ordnance Survey/EDINA supplied service. 127

Figure 4-38. Map showing locations of photogrammetry study area at Penlee Quarry with photographic overlay for detail. © Crown Copyright/database right 2009. An Ordnance Survey/EDINA supplied service. © 2009 Google, Map Data © 2009 Tele Atlas, © 2009 Getmapping plc.	128
Figure 4-39. Schematic diagram showing the set up method used to test baseline to face ratio setup variations.	129
Figure 4-40. Graph showing the average pole vector difference and standard deviation of each photogrammetric setup baseline ratio.....	130
Figure 4-41. Schematic diagram showing the set up method used to test baseline to face angle variations.	132
Figure 4-42. Graph showing the average pole vector difference and standard deviation of each photogrammetric setup with varying baseline to face angle (linear best fit line applied).....	133
Figure 4-43. Map of East Cornwall, UK, showing location of Blackpool Pit - Imerys. © Crown Copyright/database right 2009. An Ordnance Survey/EDINA supplied service.	134
Figure 4-44. Map showing locations of laser scanner setup positions at Blackpool Pit. © Crown Copyright/database right 2009. An Ordnance Survey/EDINA supplied service.	134
Figure 4-45. 3D model of one point cloud of Blackpool Pit, Imerys, St Austell, Cornwall, UK looking west. Each bench is ~15 m high. The reflectance intensity is represented as a green colour indicating a good reflectance, ranging to red for poor reflectance.	135
Figure 4-46. Map of East Cornwall, UK, showing location of Delabole Quarry. © Crown Copyright/database right 2009. An Ordnance Survey/EDINA supplied service.	136
Figure 4-47. Map showing locations of photogrammetry camera and control point setup positions at Delabole Quarry. © Crown Copyright/database right 2009. An Ordnance Survey/EDINA supplied service.....	137
Figure 4-48. 3D image showing the 1967 failure plane (highlighted red), Delabole Quarry, Cornwall, UK. It is considered that there has been little change in the slope profile since there has been no significant failure subsequently in this regularly monitored face. The camera positions had restricted views of the lower half of the pit slope, so only the upper part, which includes the failure surface, was modelled.	138
Figure 4-49. Comparison between the cross section of the 3D photogrammetric failure face (140 m and 190 m AOD) and the estimated original quarry profile (50 m – 200 m AOD), after Clover (1978).	139

Figure 4-50. Photograph of the 1967 failure face at Delabole Quarry viewed NNW, with the town of Delabole in the background. The slope is ~100 m high from the haul road.	140
Figure 4-51. Map of West Cornwall, UK, showing location of Camborne School of Mines - Test Mine. © Crown Copyright/database right 2009. An Ordnance Survey/EDINA supplied service.	141
Figure 4-52 . Point cloud of side wall within CSM Test Mine (2.5 m high). The footprint of scanner comes to the base of the rock face when ~1.5 m away from the face.....	142
Figure 4-53. An example of the multiple 3D images created of side walls and drives within CSM Test Mine. (2.5 m in height, and 3.5 m wide).....	143
Figure 4-54. Two images showing how the image of the obstruction (lamp post) is smoothed to the rock face. Some distortion has occurred between the yellow sign and the rock face, but it is minimal and does not affect the rest of the 3D model.	145
Figure 4-55. Point cloud image showing ghost points created by vehicles passing in front of laser scanner. The rock face is ~3 m high.....	146
Figure 4-56. Points within laser scanned cloud formed due to reflectance from puddle in the floor at CSM Test Mine (2.5 m tall drive, viewed east) (highlighted red).	147
Figure 4-57. Rock meshed face at excavation near Dielette, northern France (only discontinuity traces shown). The rock mesh has been bolted and closely follows to the rock face. Discontinuity orientations and discontinuity trace lengths from 68 features were successfully extracted from the ~3 m high, east - west striking model.....	148
Figure 4-58. Frequency graph showing line lengths collected from rock meshed face. The majority of the 1 m - 2 m discontinuities are sub vertical, while the longest are orientated at 35°.	148
Figure 4-59. Graph showing the percentage of features compared to those mapped in the 3D model at 90° baseline to face angle for models with decreasing baseline to face angles. At 90° - 60° to the face no discontinuity features were missed/blinded, although the number of planes that had to be mapped as discontinuity traces increased to 35%. At a 30° angle to the rock face, the number of blinded features increases to 8% at the expense of the planes (decreasing from 65% to 55%, with a 2% increase in discontinuity traces). At a 15° angle from the study face, 46% of features are blinded, where planes and discontinuity traces combined only make up 54%.	150
Figure 4-60. Evidence of dust particles picked up during laser scan at CSM Test Mine (highlighted red, 3 m high face).....	154
Figure 4-61. Field times comparison between photogrammetry, laser scanning and traditional mapping (100 fractures). Similar time is taken between the three mapping	

techniques for the preliminary stages, where the data capture/fracture measurement stage of remote mapping is ~8 times quicker than traditional mapping.	155
Figure 4-62. Geared camera head fitted with tribrach attachment (highlighted in red). The screw fitting for the geared head was modified so that it may be interchanged between normal photographic tripods and surveying tribrachs.....	159
Figure 5-1. Process work-flow diagram - indication of sections covered in Chapter 5 (red box).....	168
Figure 5-2. Map of West Cornwall, UK, showing location of Tremough Campus road cutting. © Crown Copyright/database right 2009. An Ordnance Survey/EDINA supplied service.....	169
Figure 5-3. Map showing layout of photogrammetric and laser scan setup positions, Tremough, Cornwall, UK. © Crown Copyright/database right 2009. An Ordnance Survey/EDINA supplied service.	170
Figure 5-4. Image showing blocky nature of the granite rock mass at the Tremough Campus road cutting (3 m wide, 2.5 m high rock face, looking south).....	171
Figure 5-5. Comparison between photogrammetric mesh (top) and point cloud (bottom) taken from Tremough Driveway (view orientated SE).	174
Figure 5-6. Lower hemisphere stereonet showing photogrammetrically captured orientation data.....	175
Figure 5-7. Lower hemisphere stereonet showing laser scanning captured orientation data.	175
Figure 5-8. Lower hemisphere stereonet showing hand-mapping captured orientation data.	175
Figure 5-9. Pole vector difference for remotely captured data compared with hand-mapped orientation as a function of area of the identified fracture plane (measured using photogrammetry). Plotted on log-log axes.	177
Figure 5-10. Stereonet showing set analysis on hand-mapped data.	179
Figure 5-11. Stereonet showing set analysis on photogrammetrically mapped data.	179
Figure 5-12. Stereonet showing set analysis on laser scanned mapped data.	179
Figure 5-13. Above: 2D orthoimage with discontinuity trace and plane highlighted red. Below: corresponding 3D image showing plane fitted to discontinuity trace.....	180
Figure 5-14. Tracelength identification using window mapping from a digital photograph, Tremough Road cutting, Penryn, Cornwall (3 m wide, 2.5 m high rock face, looking south). The discontinuity traces are coloured according to orientation to the rock face. Shaded areas indicate the planes from which the traces are delineated.	182

Figure 5-15. Photogrammetric discontinuity trace length identification, Tremough Road cutting, Penryn, Cornwall, UK (~3 m wide, 2.5 m high rock face, looking south).	183
Figure 5-16. Photogrammetric and traditionally mapped discontinuity trace length frequency distribution. Both are positively skewed normal or log normal distributions, although there is some variation in the larger ranges for both photogrammetric and traditional mapping techniques. On average the photogrammetric discontinuity trace lengths were shorter than the traditionally mapped features, 0.54 m and 0.61 m respectively.....	184
Figure 5-17. Hand-mapped JRC plotted against photogrammetrically mapped RMS showing a weak positive trend.	186
Figure 5-18. Hand-mapped JRC plotted against photogrammetrically mapped variance showing a weak negative trend.....	186
Figure 5-19. Hand-mapped JRC plotted against laser scanned roughness showing a weak negative trend.....	186
Figure 5-20. Measurement of joint roughness (from Wyllie & Mah, 2004, modified from Tse & Cruden, 1979).	188
Figure 5-21. Photogrammetric 3D image showing partition of large box (7.6 m ²) into smaller boxes, 4 x 1.9 m ² , 16 x 0.475 m ² and 64 x 0.119 m ² , Tremough Campus Road cutting, Penryn, Cornwall, UK, looking SSE.....	189
Figure 5-22. Stereonet and zoomed section showing photogrammetric poles (blue), laser scanned poles (yellow) and hand-mapped poles (red) (average shown in green).	190
Figure 5-23. Pole vector difference of photogrammetry at varying box areas from average orientation taken from total plane area. It shows that the range of the pole vector differences from the total plane orientation reduces as the size of the plane measured increase.	191
Figure 5-24. Pole vector difference of laser scanning at varying box areas from average orientation taken from total plane area. Mirroring photogrammetry; the graph shows that the range of the pole vector differences from the total plane orientation reduces as the size of the plane measured increase.	191
Figure 5-25. Process work-flow diagram for geotechnical end-uses.....	194
Figure 5-26. Map showing locations of laser scanner setup position at Saltdean. © Crown Copyright/database right 2009. An Ordnance Survey/EDINA supplied service.	196
Figure 5-27. Swedge back-analysis on fallen wedge, data collected from laser scanned point cloud at Saltdean, Brighton, UK. The ~18 m high cliff has been scaled	

for loose blocks and has had a buttress installed to increase stability and to act as a catchment for small rockfall (~1.5 m ³).	196
Figure 5-28. AutoCAD (Autodesk, 2008) 3D representation of blocks formed from virtual scanline spacing data (from Saliu, 2009).	197
Figure 5-29. Example circular window mapping from orthoimage of Carnsew Quarry (lower circles 6 m diameter, upper circles 10 m diameter). Using an orthoimage removes the perspective bias of using normal photographs. The circles were scaled using ImageJ (Rasband, 2007) and superimposed onto the orthoimage showing the discontinuity traces coloured according to orientation.	200
Figure 5-30. Process work-flow diagram for end-uses using digital elevation model data.	204
Figure 5-31. Point cloud image showing 2D profile section highlighted in red, Saltdean, Brighton, UK. The ~18 m high cliff has been scaled for loose blocks and has had a buttress installed to increase stability and to act as a catchment for small rockfall. ...	205
Figure 5-32. Simulated RocFall scenario showing rock fall paths from the cliff profile taken of Saltdean, Brighton, UK. The profile was constructed from a reduced number of points from the laser scanned point cloud as too many were imported for the RocFall program to compute without problems.	206
Figure 5-33. 3D mine map from laser scanned point cloud showing drives and collapsed stope (30 m wide approx). The grey indicates the interior surface of the mine, where the blue indicates the exterior.	208
Figure 5-34. Process work-flow diagram for end-uses using visual data.	210
Figure 5-35. Images showing colour recognition. The top image shows the four points from which the colour range is chosen. The bottom image shows the areas of the face that match the colour from selected range.	211
Figure 6-1. Diagram showing stereonet overlay indicating areas of precision for remote data capture systems (viewing along a horizontal plane and from one setup position). The highest precision is achieved for features that are near perpendicular to the viewing angle. As features become more oblique in both the horizontal and vertical planes then the precision decreases.	220
Figure 6-2. Ideal work-flow diagram (with key underneath). The process work-flow is more simplified whilst each mapping technique can assess multiple rock mass characteristics.	225
Figure 7-1. Venn diagram showing individual and shared advantages between hand and remote mapping techniques to capture rock mass characteristics.	231

LIST OF TABLES

Table 3-1. Field estimates of uniaxial compressive strength (from Hoek & Brown, 1997). Qualitative empirical descriptions of rock strength in the field can be used to roughly estimate the quantitative value.	52
Table 3-2. Weathering grades (from ISRM, 1981b). Using descriptions of the rock mass the grade of weathering can be estimated for use in subsequent analysis.	53
Table 3-3. Comparison of techniques used in measurement of joint surface roughness (from Unal, 2000). The table suggests that both digital photogrammetry and laser scanning are well suited for roughness measurements.....	55
Table 3-4. Example of spreadsheet calculating positional XYZ coordinates from particular data inputs. Inputs include the angles and distances to each camera and controls point. Triangulation calculations are used to estimate the unknown locations.	59
Table 3-5. Sirojoint reliability measure (CSIRO, 2005). Inaccuracies may be produced during matching, where points had to be interpolated from surrounding accurate matched points.	77
Table 4-1. Calculation of pole vector error between five hand-mapped discontinuities and the corresponding measurements made using remote mapping techniques. Arrows indicate direction of calculations.	90
Table 4-2. Locations of photogrammetry camera and control point setups at Portobello, Brighton, UK, indicating model scale and lens used.....	96
Table 4-3. Locations of laser scanner setup positions at Portobello, Brighton, UK, also indicating the scan density used.	99
Table 4-4. Orientations of contour highs found from the differing remotely mapped 3D models and from hand-mapping. Corresponding sets have been sorted next to one another for comparison.	102
Table 4-5. Orientations of contour highs compared using pole vector differences across the large scale data captured by photogrammetry, laser scanning and hand-mapping. Only comparable sets were used.	104
Table 4-6. Locations of photogrammetry camera and control point setups at Gwithian, Cornwall, UK, indicating model and lens used.	107
Table 4-7. Locations of photogrammetry camera and control point setups at Gunwalloe, Cornwall, UK, indicating model and lens used.....	111
Table 4-8. Locations of laser scanner setup positions at Portreath, Cornwall, UK, also indicating the scan density used.	113

Table 4-9. Locations of photogrammetry camera and control point setups at Porthgwarra, Cornwall, UK, indicating model and lens used.	117
Table 4-10. Locations of laser scanner setup positions, and photogrammetry camera and control point setups at Carn Marth Quarry and Theatre Quarry, Cornwall, UK, indicating model, lens and scan density used.	122
Table 4-11. Table showing the set analysis for each remote mapping model and hand-mapping. Six sets were identified across the two quarries. Set one from the Theatre Quarry was split into A and B (steeply and shallow dipping subdivisions).	124
Table 4-12. Pole vector difference analysis on data collected from northern section of Carn Marth Quarry.	125
Table 4-13. Assessment of remote data capture systems to collect data from varying rock structures (modified from Marinos & Hoek, 2000).	126
Table 4-14. Locations of photogrammetry camera and control point setups at Porthgwarra, Cornwall, UK, indicating camera separation, baseline ratio and lens used.	129
Table 4-15. Example table showing pole vector differences (PVD) between hand-mapping and photogrammetric mapping with varying baseline ratios.	130
Table 4-16. Locations of photogrammetry camera and control point setups at Porthgwarra, Cornwall, UK, indicating camera separation, baseline orientation to face and lens used.	131
Table 4-17. Locations of laser scanner setup positions at Blackpool Pit - Imerys, Cornwall, UK, also indicating the scan density used.	135
Table 4-18. Locations of photogrammetry camera and control point setups at Delabole Quarry, Cornwall, UK, also indicating lens used.	137
Table 4-19. Locations of laser scanner setup positions, and photogrammetry camera and control point setups for testing laser scanning blinding, indicating model, lens and scan density used.	151
Table 4-20. Results of blinding effects on laser scanning. The single laser scan only captured 86% of the features mapped using photogrammetry, had a pole vector difference of $\sim 18.83^\circ$ from hand-mapping and a standard deviation of 16.18° . The three combined laser scans were able to capture 13% more features than the single scan whilst obtaining a 11.96° pole vector difference from hand-mapping. The standard deviation was reduced by 40% to 9.6°	152
Table 4-21. Comparison of each positioning technique from experience during study (Additional data sourced: Leica, 2005; CG Surveying Ltd, 2007; RICS, 2007).	156
Table 5-1. Locations of photogrammetry camera and control point setups at the Tremough Campus road cutting, Cornwall, UK, indicating model and lens used.	172

Table 5-2. Locations of laser scanner setup positions at the Tremough Campus road cutting, Cornwall, UK, indicating the model and scan density used.....	173
Table 5-3. Number of planar features identified using each mapping technique.....	173
Table 5-4. A comparative table showing the average pole vector difference and standard deviation between each mapping technique. Data has been split into discontinuities dipping below and above 47°.....	176
Table 5-5. Set analysis for comparative data collected from Tremough Road Cutting. Each mapping technique is compared with one another. Fisher K and number of poles within each set are included in the set statistics.....	178
Table 5-6. Plane and discontinuity trace pole vector differences from hand-mapping.	181
Table 5-7. Photogrammetric and traditionally mapped discontinuity trace lengths frequency and frequency percentage.....	183
Table 5-8. Example roughness measurements taken from the Tremough road cutting.	185
Table 5-9. Correlation (R) and 95% confidence values of remotely mapped roughness measurements with hand-mapped JRC measurements.....	185
Table 5-10. Conversion of remotely mapped roughness measurements to JRC values developed from measurements taken from the Tremough Road Cutting.	187
Table 5-11. Table showing the pole vector difference between spot hand-mapped data taken from the study plane and the average plane orientation measured from the entire area by photogrammetry and laser scanning.	192
Table 5-12. By using the superimposed circles on the orthoimage, the discontinuity trace count for circular window mapping can be completed and split according to each set.	201
Table 5-13. Using the methodologies developed by Zhang & Einstein (1998); Zhang & Einstein (2000); La Pointe (2002); and Zhang <i>et al.</i> (2000) the mean fracture radius and standard deviation for each set and probabilistic distribution type can be calculated.	201
Table 5-14. Assessing the ability of photogrammetry and laser scanning to calculate parameters from RMR, Q system and GSI rating systems.....	203

ACKNOWLEDGEMENTS

I would like to thank my supervisors, Professor Robert Pine and Professor John Coggan for their continual help and guidance during the PhD project. Their wide knowledge, ideas, and logical way of thinking have been of great value to me during this project and will be with me throughout my future career.

My colleagues in the Camborne School of Mines PhD Room provided me with a friendly working environment and were always willing to help with many aspects of my project, specifically Muyideen Saliu and Dr Zara Flynn, who both assisted me with hand-mapping on certain field trips. I would also like to thank Dr Andrew Wetherelt who undertook the laser scanning fieldwork with me and taught me how to use the Leica hardware and software. Steve Pendray helped with the modifications to the equipment used during the project.

Also thanks to the rest of the CSM staff, all of whom helped me through my undergraduate degree at the old campus in Camborne during lectures and numerous field trips, they then continued to give helpful input and made constructive comments during my PhD study.

During the later stages of writing up my thesis SRK Consulting UK Ltd provided me with time and resources to help me finish my final corrections.

I would also like to thank my family; my brothers Tom and Leo, and my parents, Alec and Serena for their encouragement and support throughout my time at Camborne.

I would not have been able to complete the PhD without Emma. Thank you for your constant love, patience and understanding.

The location maps were accessed from the Digimap Ordnance Survey Collection (© Crown Copyright/database right 2009. An Ordnance Survey/EDINA supplied service) and via Google Earth (© 2009 Google, Map Data).

Financial support has been provided by the European Social Fund.